

PROCEEDINGS OF SPIE

[SPIDigitalLibrary.org/conference-proceedings-of-spie](https://www.spiedigitallibrary.org/conference-proceedings-of-spie)

Multiple guide star tomography demonstration at Palomar Observatory

V. Velur, R. C. Flicker, B. C. Platt, M. C. Britton, R. G. Dekany, et al.

V. Velur, R. C. Flicker, B. C. Platt, M. C. Britton, R. G. Dekany, M. Troy, J. E. Roberts, J. C. Shelton, J. Hickey, "Multiple guide star tomography demonstration at Palomar Observatory," Proc. SPIE 6272, Advances in Adaptive Optics II, 62725C (27 June 2006); doi: 10.1117/12.671666

SPIE.

Event: SPIE Astronomical Telescopes + Instrumentation, 2006, Orlando, Florida , United States

Multiple guide star tomography demonstration at Palomar observatory

V. Velur^a, R. C. Flicker^b, B. C. Platt^c, M. C. Britton^a, R. G. Dekany^a, M. Troy^c, J. E. Roberts^c, J. C. Shelton^c, J. Hickey^d

^aCalifornia Institute of Technology, Pasadena, CA 91125, USA;

^bW. M. Keck Observatory, Kamuela, HI 96743, USA;

^cJet Propulsion Laboratory, 4800 Oak Grove Drive, Pasadena, CA 91109, USA

^dPalomar Observatory, 35899 Canfield Rd., Palomar Mountain, CA 92060-0200, USA.

ABSTRACT

We have built and field tested a multiple guide star tomograph with four Shack-Hartmann wavefront sensors. We predict the wavefront on the fourth sensor channel estimated using wavefront information from the other three channels using synchronously recorded data. This system helps in the design of wavefront sensors for future extremely large telescopes that will use multi conjugate adaptive optics and multi object adaptive optics. Different wavefront prediction algorithms are being tested with the data obtained. We describe the system, its current capabilities and some preliminary results.

Keywords: Multi-Conjugate adaptive optics, tomography, novel wavefront sensing

1. INTRODUCTION

The Palomar tomograph (PT) is a compact multiple guide star wavefront sensor system that can be used to test different tomographic wavefront sensing algorithms.¹ The implementation and performance characterization of these algorithms will be the driving force for wide field adaptive optics (AO) and in turn AO fed spectroscopy. This is a key technology development effort for the next generation of AO systems on 8-10m class telescopes and for the planned Thirty Meter Telescope (TMT) and the Giant Magellan Telescope (GMT) projects^{3 6 5 .8}. Using PT we are comparing different algorithms and assessing the importance of a priori turbulence statistics. Slope detection and ranging (SLODAR) experiments to determine the heights of strong turbulence layers are also being performed using cross-correlation of wavefront sensor data obtained.² Palomar currently has a multi-aperture scintillation sensor and a differential image motion monitor (MASS and DIMM unit), on loan from the TMT project office, which enables us to monitor and characterize the atmospheric turbulence concurrent with our PT observations.

2. SYSTEM DESCRIPTION:

Five low noise CCD based Shack Hartmann wavefront sensors have been integrated into the existing the Palomar Adaptive Optics (PALAO) bench. The five wavefront sensors consist of three 16x16 sub-aperture channels and one 3x3 sub-aperture low order wavefront sensor (LOWFS) inside the PT enclosure and one 16x16 Active High Order Wavefront Sensor (AHOWFS) outside the enclosure that receives light from a small reflective field stop. The three 16x16 wavefront sensors inside the enclosure read out 64x64 pixels with 4x4pixels/sub-aperture while the AHOWFS reads out 64x64 pixels that are binned on chip to provide 32x32 active super-pixels. The LOWFS has 27x27 active pixels that are binned 3x3 to provide 9x9 active super pixels. The four wavefront sensor (WFS) channels inside the PT enclosure can traverse an almost continuous field of ~ 90 arc-seconds, while a pair of mirrors in PALAO can be moved so that the active wavefront sensor can acquire guide stars. Between these two acquisition systems, we can acquire and guide on asterisms where the maximum separation between stars is less than 90 arc-sec.

Author to whom correspondence should be sent: V. Velur - Robinson 01, Mail Code - 105-24 Caltech, 1200 E California Blvd., Pasadena, CA - 91125. E-mail: vnv@phobos.caltech.edu

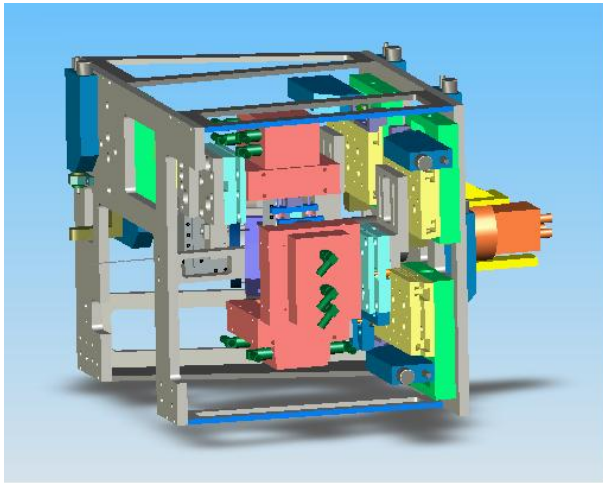


Figure 1. Three dimensional rendering of the multiple guide star tomograph showing 4 MGSU channels. Each WFS is mounted on a tip-tilt stage for accurate alignment. The tip-tilt stage itself is mounted on X and Y translation stages for picking off stars in the FoV.

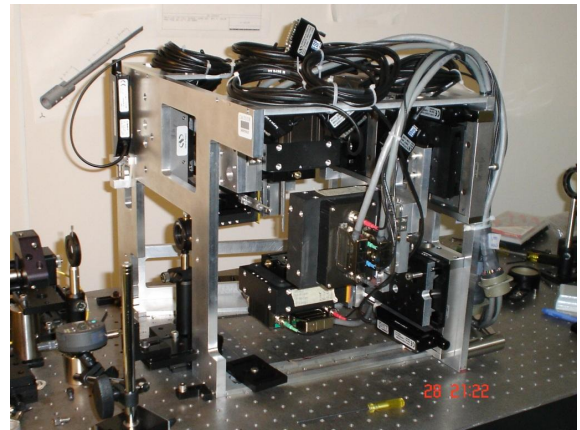


Figure 2. The Tomograph as built in the lab.

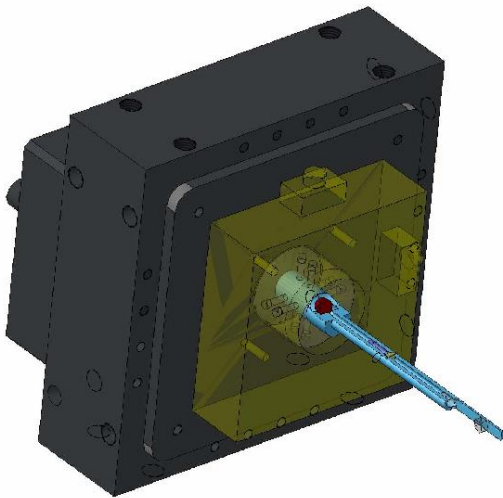


Figure 3. Depiction of a single channel of the MGSU unit with penta prism pick-off, collimator, lenslet array, relay optics and detector.



Figure 4. Shows the PT electronics rack with the 8 channel motion controller, a Windows test PC, camera controller, network power switch, four 1U Dell PCs and two RAID disks.

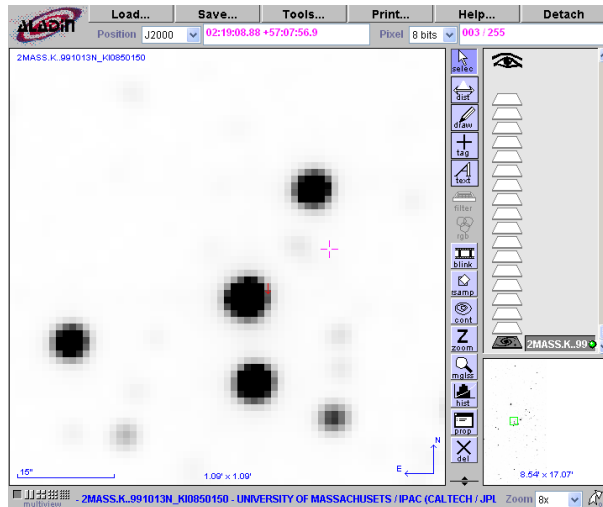


Figure 5. Asterism in Aquila (SAO23181) used for our tests. WFS data from the 3 bright stars was used to predict the wavefront from the central brightest star. The *truth* sensor was the PALAO high order WFS which was also used to close the tip-tilt loop of the AO system.

All five wavefront sensors use cameras and controllers made by SciMeasure Analytical Systems, Inc. (SAS) that grab frames at a maximum rate of 2000 Hz when running in 64x64 pixel read out mode. These cameras have a measured $3e^{-}s/sec$ read noise at 500 Hz and the noise level creeps up to $7e^{-}s/sec$ at 2000 Hz. The LOWFS serves as our tip, tilt, focus and astigmatism sensor for Laser Guide Star (LGS) operations and does not play a part in the tests described.

PT's pick off arms can traverse an almost continuous field of 90 arc-sec. diameter to acquire guide stars. The optical train is designed to be telecentric over this range to keep pupil shear to within 1.2% at the lenslet pupil over this field of view. The system can be operated with PALAO's tip-tilt and high order AO loop closed, with both open or with just the tip-tilt loop closed. A custom timing module is used to trigger the wavefront sensing channels to run at integral frame rates of a master trigger as shown in Figure 6. This facilitates use of the system with guide stars of different magnitudes. Different program selections are available on the SAS cameras to enable data to be recorded at frame rates between 50-2000 Hz. The 14 bit, 64x64 pixel data from the channels inside the enclosure and 14 bit 32x32 on-chip binned pixel data from the AHOWFS are recorded onto two striped RAID disks with 3.2 Terabytes of storage space.

3. SIMULATION AND DATA ANALYSIS ALGORITHM DEVELOPMENT

3.1. Description of the experiment

The general scope of the experiment is to use the information from three natural guide stars (NGS) to estimate the wavefront at a fourth position, where a fourth NGS is available to provide a *truth* measurement. Performance is assessed by comparing the truth measurement against the prediction from the three NGSs. The simplest asterism for this type of estimation and validation would be to have three stars at the vertices of an equilateral triangle that feed the tomography sensors and a fourth star at the centroid serving as the truth sensor. We use the AHOWFS of the PALAO system on the central star to act as truth sensor, and the three MGSU cameras on the surrounding stars act as the tomographic WFSs. A variation of this experiment may be carried out using only three NGSs, where two are employed to make a prediction for the third, which may be located off-axis rather than in the central region. This variant of the original experiment mimics the situation in certain MOAO (multi-object adaptive optics) designs or to sharpen an off-axis tip-tilt NGS based on on-axis LGS tomography.

Given simultaneous measurements from four WFSs on a 4-star asterism as described above, one can apply a number of different analysis methods that will answer a variety of questions about the data set and the outcome

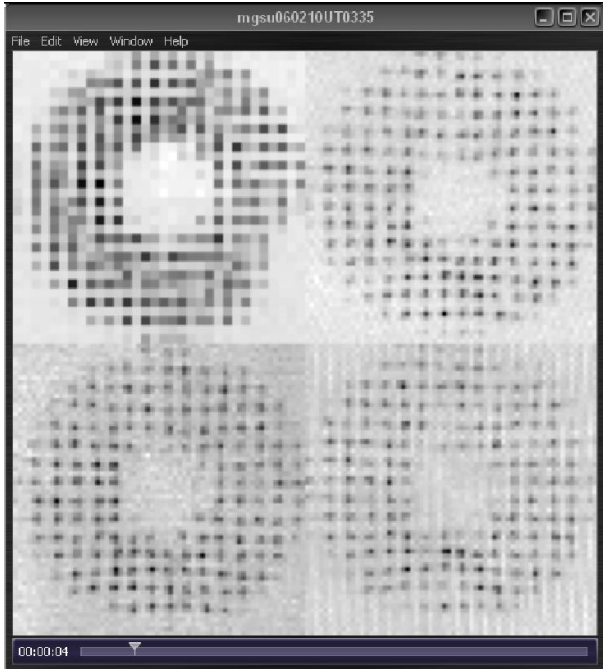


Figure 7. Image showing a single frame of on-sky data from each of the four WFS channels. In this case, the tip-tilt loop was locked using the high order wavefront sensor (32x32 sub-aperture), and the other 3 cameras were recording data in 64x64 mode.

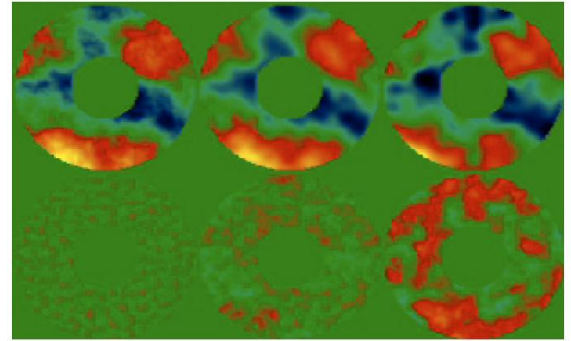


Figure 8. Sample simulation result screen from main IDL analysis code. Top row - wavefronts: pure open loop turbulence (left); HOWFS reconstructed wavefront (center), and MGSU reconstructed wavefront (right). Bottom row - residual wavefront errors w.r.t. the true wavefront: optimal fit of 17x17 actuator DM (left); HOWFS reconstructed wavefront error (center); MGSU reconstructed wavefront error (right).

were centered and the sub-apertures aligned. Then we unlocked the tip-tilt loop, and began the data acquisition. After a few seconds of data acquisition the tip-tilt loop was locked to keep the images on each of the detectors stable. The DM loop was locked for the last minute of the exposure. Data was recorded at a few different frame rates ranging from 60 to 256 Hz (limited by guide star magnitude). Figure 9 shows our observation log and includes information about the asterism we observed. A sample frame from this data taken is shown in figure 7.

4.1. Analysis implementation and preliminary results

The data analysis is distributed over various existing codes and additional code developed for this experiment. The wavefront reconstruction matrices were generated using the Yorick Adaptive Optics (YAO) simulation code⁷ modified specifically for MGSU simulations. Figure 12 shows sample initial results for estimating the wavefront w from the vector v of MGSU measurement, obtained through the following linear estimation steps:

$$w = HG^+\hat{u}, \quad (1)$$

$$\hat{u} = Ev, \quad (2)$$

where G^+ is the pseudo-inverse of a simulated interaction matrix for the AHOWFS, and H is a set of influence functions. Both were modeled in YAO. E is the statistical least-squares tomographic estimator:

$$E = \langle uv^t \rangle \langle vv^t \rangle^{-1}, \quad (3)$$

where u is the on-axis (AHOWFS) centroid vector. Figure 8 shows a sample frame from a YAO simulation that was completed prior to the on-sky experiment in order to assess what we may expect from the real data.

Experiment #	3	Asterism #	A1
Date/time	2006-02-10	RA (J2000)	02:19:10
UT	03:35	DEC (J2000)	+57:07:50
FSM loop	closed	ZD/airm	1.27 airm
DM loop	open	Cass ring	205.32 deg

	HOWFS	MGSU 2 (Chico)	MGSU 3 (Zeppo)	MGSU 4 (Harpo)
format	32x32	64x64	64x64	64x64
program/cfg.	5/Lil-Joe-32x32	5/Lil-Joe-64	5/Lil-Joe-64	5/Lil-Joe-64
d. frame rate	256	256	256	256
gain	2	0	0	0
star name	SAO 23181	BD+56 526	BD+56 529	BD+56 525
magnitude	8.43 V	8.98 V	10.21 V	9.24 V
exposure time	308.075			
frame rate	256.064			
# frames	78887			

Figure 9. Observing log showing the star brightnesses and camera speeds for one data set.

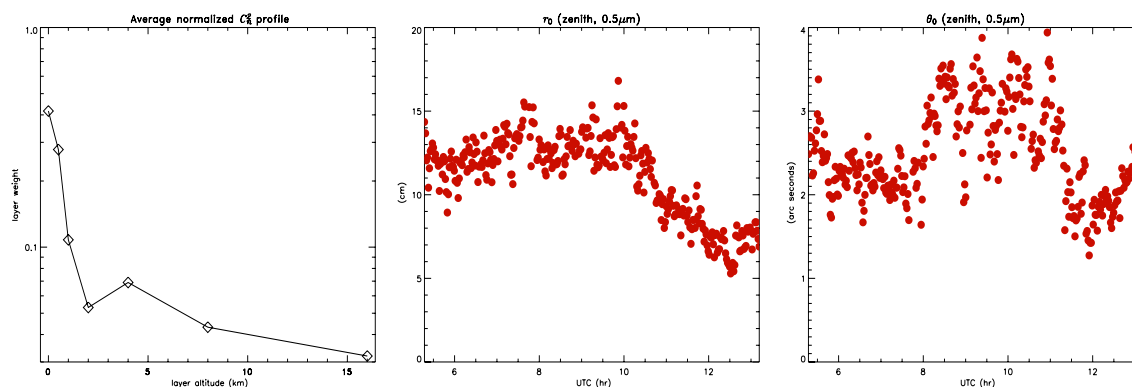


Figure 10. The top left image shows the C_n^2 profile averaged over the night for 7 layers of the atmosphere. Center and right images show the time evolution of the isoplanatic angle and the Fried parameter.

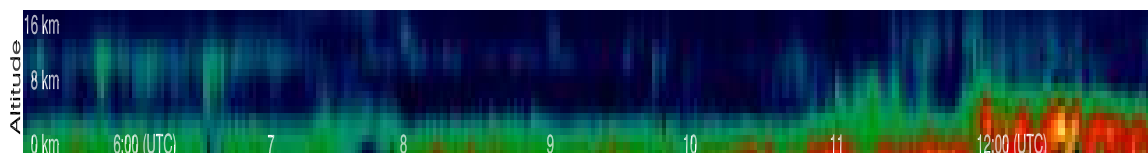


Figure 11. Time evolution of C_n^2

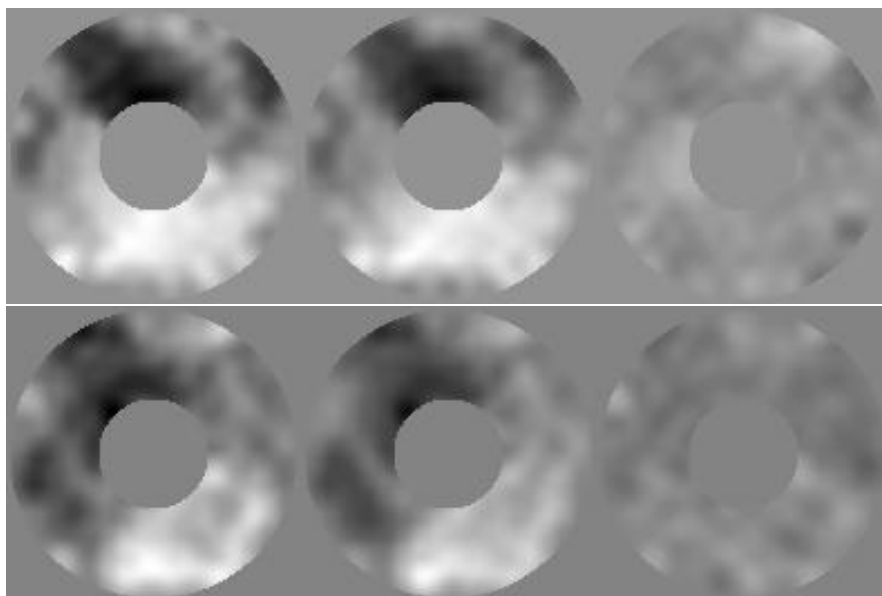


Figure 12. Two sample analysis frames from the 10 February 2006 data set, with the tip-tilt loop closed on the HOWFS. Left column: wavefronts reconstructed directly from HOWFS (*truth* wavefront). Center column: wavefronts estimated from MGSU measurements. Right column: residual wavefronts.

Figure 12 shows a sample analysis frame from the data set taken on 10 February 2006. The value of r_0 and θ_0 were obtained from the MASS DIMM measurements. The variation of r_0 and θ_0 during the night is shown in Figures 10 and 11.

We estimated a Fried parameter of $r_0 \approx 10$ cm from the MASS/DIMM unit during the above five minute exposure. Kolmogorov theory suggests that a $r_0 = 10$ should produce a tip/tilt-removed RMS wavefront error of 759 nm over a 5-m aperture. The central obscuration of the Hale telescope and the high-spatial frequency cut-off of the AHOWFS (estimated at $1/31.2 \text{ cm}^{-1}$) lowers the Kolmogorov predicted RMS wavefront error to 671 nm.

From the wavefronts reconstructed directly from the AHOWFS (left column of Figure 12), we estimate for this data set an RMS wavefront error of 598 nm (left column of Figure 12). Figure 13 shows that most of the discrepancy is in the low-order modes, which in our estimation has a lower variance the Kolmogorov statistics would predict. Using 40,000 frames of this data set, we measure an RMS error in the tomographic wavefront estimation of 231 nm (right column of Figure 12), when using the statistical least-squares estimator in equations (1)-(3). Currently, our results from this preliminary estimate are limited by the following:

- Noise in the WFS camera that was gathering data from the faintest star.
- Internal calibration errors, pupil registration, telecentricity (we have not yet measured the actual pupil shear across the pupil) and cross talk between sub-apertures.
- The use of the statistical least-squares tomographic estimator, which may be significantly non-optimal. Modeled maximum a posteriori estimators are being constructed and will be applied to the data sets in the next phase of the analysis.

A more rigorous analysis is underway to quantify the errors in our tomographic estimation.

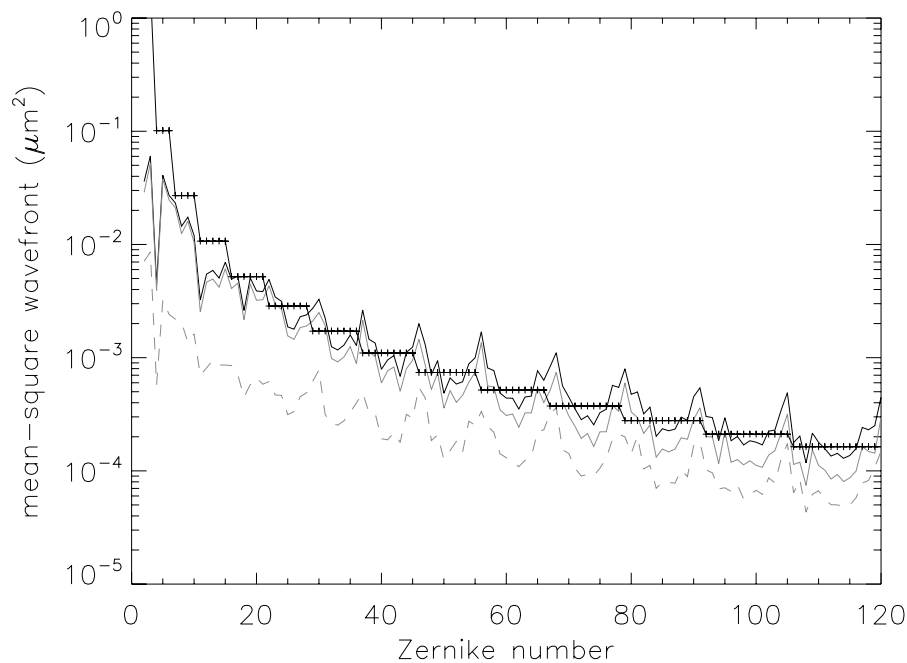


Figure 13. Zernike coefficients from estimated wavefronts (fitted with a central obscuration). Plotted are the estimated RMS wavefront errors for the HOWFS direct reconstruction (solid black line), tomographic estimation (solid grey line), and the residual error (dashed grey line). For comparison is also plotted the theoretical Zernike variances for an unobscured aperture (solid black line and pluses).

5. CONCLUSION

We built and field tested a four channel tomograph unit. We estimated the wavefront error of the central star from the three surrounding ones to 231 nm RMS error using a Wallner-type estimator.

We developed a scheme to align and manufacture wavefront sensors in a batch process using special jigs that give us an understanding of how to replicate wavefront sensors for use in wide-field AO for ELTs. With more field-testing of the current system we will learn to calibrate the it better and gain knowledge on how to acquire stars quickly. This will greatly improve the observing efficiencies of large observatories and is also an issue with most single laser guide star systems.

5.1. Future Work

After gaining confidence in our tomography algorithms and optimizing them, the experiment can be refined to obtain better estimates of the wavefront at the truth sensor.

The tomographic reconstruction currently works in open loop (done in post-processing), but the system was designed with the intention of operating in closed loop with a real-time computer that drives the existing DM using wavefront information obtained from all WFSs. The ELTs require tomographic WFSs operating in real time.

The Caltech, JPL and The University of Chicago PALAO team is currently planning a major upgrade of existing Laser Guide Star (LGS) AO system. Firstly, we are upgrading our 241 active element AO system to a 3000 active element system.⁹ As a second step we are upgrading the laser in our LGS system from a 8.5W to a 20W system. Lastly, an optical integral field spectrograph designed to take advantage to the nearly diffraction limited Point Spread Functions (PSFs) produced by PALAO called Oxford Short Wavelength Integral

Field Spectrograph (OSWIFT) is being built by Oxford University, U.K. to go behind the PALAO. A variety of experiments and use for the MGSU can be devised, keeping in mind, the grand scheme of PALAO upgrades planned in the imminent future.

6. ACKNOWLEDGMENTS

This work was supported by the National Science Foundation (NSF) under Agreement No. AST-0096928, the Thirty Meter Telescope (TMT) project, W. M. Keck Observatory and internal Caltech Optical Observatories funds. The authors thank the JPL AO team and staff of Palomar Observatory for valuable support rendered at various stages of this project. Special thanks to Prof. Ed Kibblewhite (The University of Chicago) for useful insight during the design phase. We would also like to thank the TMT site-selection team and Dr. A. J. Pickles (COO) for ensuring that the MASS/DIMM unit was up and working during these experiments. In particular, the efforts of Reed Riddle, Warren Skidmore, Matthias Schöeck, Sebastian Els (CTIO) and Tony Travouillon to keep the unit in perfect running condition despite their busy TMT site survey activities.

The Thirty Meter Telescope (TMT) Project is a partnership of the Association of Universities for Research in Astronomy (AURA), the National Science Foundation (NSF), the Association of Canadian Universities for Research in Astronomy (ACURA), the California Institute of Technology and the University of California. The partners gratefully acknowledge the support of the Gordon and Betty Moore Foundation, the US National Science Foundation, the National Research Council of Canada, the Natural Sciences and Engineering Research Council of Canada, and the Gemini Partnership.

REFERENCES

1. R. Dekany, M. Troy, K. Wallace, C. Bleau, R. DuVarney, G. Motter, Multiple Guide Star Wavefront Sensing for Palomar AO, Beyond Conventional Adaptive Optics, Venice, Italy 2001.
2. L. Wang, University of California, Irvine, CA, Private communication.
3. R. Ragazzoni, E. Marchetti and G. Valente, Adaptive optics correction for the whole sky, *Nature* 403, pp 54-56
4. E.P. Wallner, Optimal wave-front correction using slope measurements, *JOSA-A*, 73, Dec. 1983, pp 1771-1776.
5. D. Gavel, Tomography for multiconjugate adaptive optics systems using laser guide stars, Vol. 5490, SPIE Glasgow 2004.
6. P. Knutsson and M. Owner-Petersen, Emulation of dual-conjugate adaptive optics on an 8-m class telescope, *Opt. Express*, 11, 2231-2237 (2003).
7. F. Rigaut, <http://www.maumae.net/yao/aosimul.html>
8. C. Baranec, B. Bauman M. Lloyd-Hart, Concept for a laser guide beacon Shack-Hartmann wave-front sensor with dynamically steered subapertures, *Optics Letters*, 30, 693-695, 2005.
9. R. G. Dekany, A. H. Bouchez, M. C. Britton, V. Velur, PALM-3000: visible light AO on the 5.1-m Telescope, submitted to SPIE Orlando 2006.